Journal of Geophysical Research: Atmospheres

RESEARCH ARTICLE
10.1029/2018JD029266

Key Points:
- Tropospheric ozone level at Mt. Happo, Japan, dropped in the late 2000s, despite increasing Chinese emissions
- Persistent La Niña-like wind pattern has reduced long-range transport from East Asia via weakened westerly winds
- Without the persistent La Niña-like wind pattern, the ozone trend over Japan would have been further upward in the late 2000s

Correspondence to:
S. Okamoto and H. Tanimoto,
okamoto.sachiko@nies.go.jp;
tanimoto@nies.go.jp

Citation:
Okamoto, S., Tanimoto, H., Hirota, N., Ikeda, K., & Akimoto, H. (2018). Decadal shifts in wind patterns reduced continental outflow and suppressed ozone trend in the 2010s in the lower troposphere over Japan. *Journal of Geophysical Research: Atmospheres*, *123*, 12,980–12,993. https://doi.org/10.1029/2018JD029266

Received 27 JUN 2018
Accepted 1 NOV 2018
Accepted article online 4 NOV 2018
Published online 20 NOV 2018

Decadal Shifts in Wind Patterns Reduced Continental Outflow and Suppressed Ozone Trend in the 2010s in the Lower Troposphere Over Japan

S. Okamoto[1], H. Tanimoto[1], N. Hirota[1], K. Ikeda[1], and H. Akimoto[1]

[1]Center for Global Environmental Research, National Institute for Environmental Studies, Tsukuba, Japan

Abstract The large increase in the springtime free tropospheric ozone over the western and eastern North Pacific over the last decades has been linked to the increase in anthropogenic emissions in China. However, the increasing trend at Mt. Happo, Japan, has been unexpectedly suppressed since 2008, by 5–10 ppbv. In this paper, we analyzed the tropospheric ozone records at Mt. Happo, along with the changes in climate and anthropogenic emissions. We revealed, based only on observational data, that the changes in climate pattern play an important role in controlling the decadal ozone trend. We found that the persistent La Niña-like wind pattern during 2008–2013 reduced the export of polluted air masses from East Asia to the western Pacific, even though Chinese emissions continued to increase. On the other hand, an El Niño-like wind pattern during 1992–1996 and enhanced storm track activity during 2000–2006 enhanced the export of polluted air masses from East Asia, contributing to the accelerated ozone trends. The climate modulations were identified in the O_3 trends at the surface sites in western and central Japan and at a remote marine boundary layer site, Minamitorishima. Without this climatic effect driven by the persistent La Niña-like wind pattern, the ozone trend would have been further upward over the North Pacific in the late 2000s to the early 2010s.

1. Introduction

Tropospheric ozone (O_3) is one of the most important trace gases in the Earth's atmosphere because it plays a central role in determining the oxidizing capacity of the atmosphere and air quality at local, regional, and global scales. As a short-lived climate pollutant, it also plays a significant role in global warming/climate change. Major sources of tropospheric O_3 have been well established to be in situ photochemical production from nitrogen oxides (NO_x = NO + NO_2), carbon monoxide (CO), methane (CH_4), and nonmethane volatile organic compounds (NMVOCs) as well as stratosphere–troposphere exchange (Monks et al., 2009).

For several decades, emissions of air pollutants, including O_3 precursors, had been rapidly increasing in East Asia, particularly due to the large contribution of China whose emissions have increased substantially accompanying the rapid economic growth until recently (Kurokawa et al., 2013). Several analyses of long-term trends of surface measurements (Chang et al., 2017; Gaudel et al., 2018) and ozonesonde data (Oltmans et al., 2013) have identified the increase of surface and free tropospheric O_3 in East Asia and ascribed their increases to the increase of precursor emissions. In addition, the transport of O_3 and its precursors from China offset almost half of the effect of domestic emission reductions in western United States during 2005–2010 (Verstraeten et al., 2015). However, several recent analyses of satellite data have reported that NO_x emissions from China may have peaked in 2011 (Duncan et al., 2016; Irie et al., 2016; Krotkov et al., 2016; Miyazaki et al., 2017).

The changes in the pattern of atmospheric circulation result in changes in the transport of O_3 and its precursors from source regions. Cuevas et al. (2013) suggested that the abrupt increase in the O_3 level after 1996 at Izaña (Canary Islands, Spain) reflected a phase shift of the North Atlantic Oscillation (NAO) from negative or neutral phases to positive phases. The changes in the atmospheric circulation pattern over the North Atlantic resulted in an increased inflow of the westerlies in the midlatitude subtropical North Atlantic, which favored the transport of O_3 and its precursors from North America. A higher frequency of storms over the North Atlantic may also induce a higher incidence of stratosphere-to-troposphere exchange processes in midlatitude. Lin et al. (2014) showed that El Niño/Southern Oscillation (ENSO) and the Pacific Decadal Oscillation (PDO) modulate the O_3-rich Eurasian airflow toward the subtropical Pacific region of the Northern Hemisphere in spring and autumn. Springtime O_3 at Mauna Loa (MLO, Hawaii, USA) has been observed to

increase under El Niño conditions and to decrease under La Niña conditions. It has been demonstrated that ENSO also modulates deep stratospheric intrusions into the western United States through its effect on the meandering of the polar jet stream (Lin et al., 2015).

However, year-by-year fluctuations of O_3 concentrations caused by short-term meteorological variability often obscure long-term trends, since meteorological conditions play an important role in the long-range transport of O_3. For example, Kurokawa et al. (2009) showed that springtime surface O_3 in the western and central part of Japan is higher than the climatological mean when the surface pressure anomaly over the North Pacific east of Japan has a large negative value, since it facilitates the continental outflow. Knowland et al. (2017) found that midlatitude storms play an important role in the horizontal and vertical distributions of trace gases, by means of a warm conveyor belt, a cold conveyor belt, and a dry intrusion. Air pollutants emitted or formed in the boundary layer can, once lifted up into the free troposphere by the warm conveyor belt within the storms, can be transported rapidly in the long range by strong westerly winds and eventually become mixed with the background composition (Dentener et al., 2010; Monks et al., 2009). In the eastern United States, the frequency of summertime midlatitude storms tracking across eastern North America at 40–50°N has strong negative correlations with the number of O_3 pollution days by reducing the number of stagnation days (Fiore et al., 2015; Leibensperger et al., 2008). The authors concluded that the decrease in midlatitude storms over 1980–2006 offset the reduction of anthropogenic emissions over that period, which may suggest that in addition to short-term variability of meteorology, large-scale climate variability could play an important role in controlling the long-term trend of O_3 in the troposphere.

O_3 has long been measured at Mt. Happo Observatory (HPO), a mountainous site in Japan. There are only a few observatories at high-altitude sites in Japan, while continuous measurements of O_3 at ground level are conducted throughout the country. Measurements at high-altitude sites facilitate the investigation of long-range transport better than measurements at low-altitude sites in boundary layer, because the lifetime of O_3 increases in the free troposphere (e.g., Dentener et al., 2010). The seasonal cycle of O_3 at HPO exhibits a maximum in spring due to photochemical activity and Asian monsoon (e.g., Okamoto & Tanimoto, 2016). The transport of O_3 and its precursors from East Asia is known to be the most efficient in spring, and substantial increases in springtime O_3 have been observed in Japan (e.g., Tanimoto, 2009) and western North America (e.g., Cooper et al., 2010). Parrish et al. (2012) showed that the O_3 at HPO remarkably increased for the period 1991–2011 in all seasons, particularly in spring (0.76 ppbv/year) and that the rate of increase decreased in all seasons. However, they mentioned that the decrease of the increasing rate was strongly caused by the variability of the last few years of data. Therefore, we updated the tropospheric O_3 record, previously analyzed for the period 1998–2006 (Tanimoto, 2009) and for the period 1991–2011 (Parrish et al., 2012), through 2016 and revisited the long-term changes in springtime (March–May) tropospheric O_3, associated with the large-scale climate variability. In this paper, we show that decadal shifts in wind patterns affect the continental outflow of O_3 to the Pacific rim region, and thus, the transboundary transport and air quality in this region are controlled by large-scale atmospheric variability as well as precursor emissions.

2. Materials and Methods

2.1. Observation

HPO is located in the mountainous area near the Sea of Japan coast (Figure 1; 36.70°N, 137.80°E, 1,850 m above sea level) and is operated by the Ministry of the Environment of Japan. It contributes to the Acid Deposition Monitoring Network in East Asia (EANET) program. While pristine air masses from the Pacific are transported to HPO during the summer monsoon, the majority of the air masses pass over East Asia, mostly over northern China (>40°N), driven by the Siberian high persistent during the winter monsoon period (Kato et al., 2002; Liu et al., 2013; Narita et al., 1999).

Starting in April 1998, O_3 measurements by ultraviolet absorption instrument have been carried out at HPO within the framework of the EANET program. Details of the measurements and quality assurance/quality control system were given in a technical report (Acid Deposition Monitoring Network in East Asia, 2013). The O_3 monitor is quality-controlled in the traceability system based on the Standard Reference Photometer (SRP) 35 maintained at the National Institute for Environmental Studies (NIES), Japan (Tanimoto et al., 2007). Briefly, the O_3 monitor is periodically referenced to a transfer standard scaled to a secondary standard. The

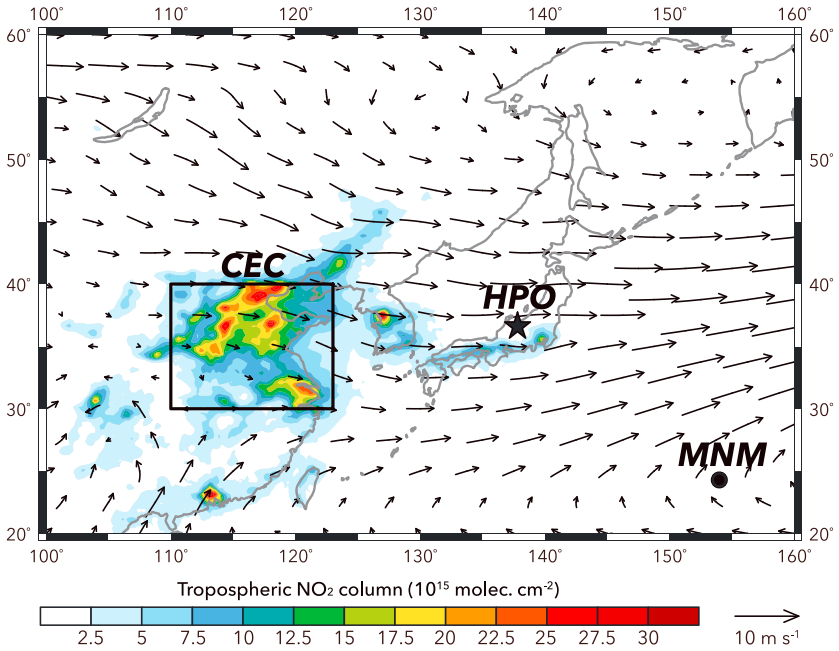

Figure 1. Map of the study area. The star shows the location of Mt. Happo Observatory (HPO), the black filled circle shows the location of Minamitorishima (MNM), and the color scale shows the distribution of the seasonal-mean tropospheric NO_2 column density from GOME-2 (METOP-A) during spring for the years 2014–2016. The black rectangle encloses the residence time analysis area in central eastern China (CEC; 30–40°N, 110–123°E). The black arrows are springtime average wind vectors (1998–2016) at 850 hPa from Japanese 55-year Reanalysis (JRA-55).

secondary standard is further scaled to a primary standard, the SRP 35. The accuracy of the O_3 monitors shall be maintained within ±5% at the level of 200 ppbv. We set up another ultraviolet absorption instrument for measuring O_3 concentrations in July 2013 to be complement each other, and both data were used in the present analysis. Our O_3 monitor was directly scaled to the SRP 35 once a year. In this study, the springtime data in 1998 and 2010 were excluded because of insufficient number of days for measurements and instrument troubles, respectively.

2.2. Emission Inventories and Satellite Observations

To examine the O_3 changes driven by the changes in the O_3 precursors emissions, we utilized emission inventories and satellite observations. The Regional Emission inventory in ASia version 1.1 (REAS 1.1; Ohara et al., 2007) and version 2.1 (REAS 2.1; Kurokawa et al., 2013) are year-dependent bottom-up inventories for major air pollutants and greenhouse gases during 1980–2003 and during 2000–2008, respectively.

Tropospheric NO_2 columns observed from space were also used to infer the spatial distributions and temporal variations of NO_x emissions in continental areas upwind of HPO. We utilized monthly mean tropospheric NO_2 column data from multiple satellite observations: GOME (Global Ozone Monitoring Experiment) for the period 1996–2003, SCIAMACHY (Scanning Imaging Absorption Spectrometer for Atmospheric Chartography) for the period 1996–2003, GOME-2 (METOP-A) for the period 2002–2016, and GOME-2 (METOP-B) for the period 2013–2016, which are available on the Tropospheric Emission Monitoring Internet Service (TEMIS; http://www.temis.nl) with detailed error estimates (Boersma et al., 2004).

2.3. Residence Time Analysis

To examine the origins and transport pathways of large-scale air masses arriving at HPO, 5-day backward trajectories were calculated using the National Oceanic and Atmospheric Administration (NOAA) Hybrid Single-Particle Lagrangian Integrated Trajectory (HYSPLIT, Version 4) model (Draxler, 1999; Draxler & Hess, 1997, 1998; Stein et al., 2015), driven by output from the Global Data Assimilation System (GDAS) meteorological model for 2005–2016 (1° × 1° grid), the Final Analysis Data (FNL) for 1997–2004 (1° × 1° grid), and National Centers for Environmental Prediction/National Center for

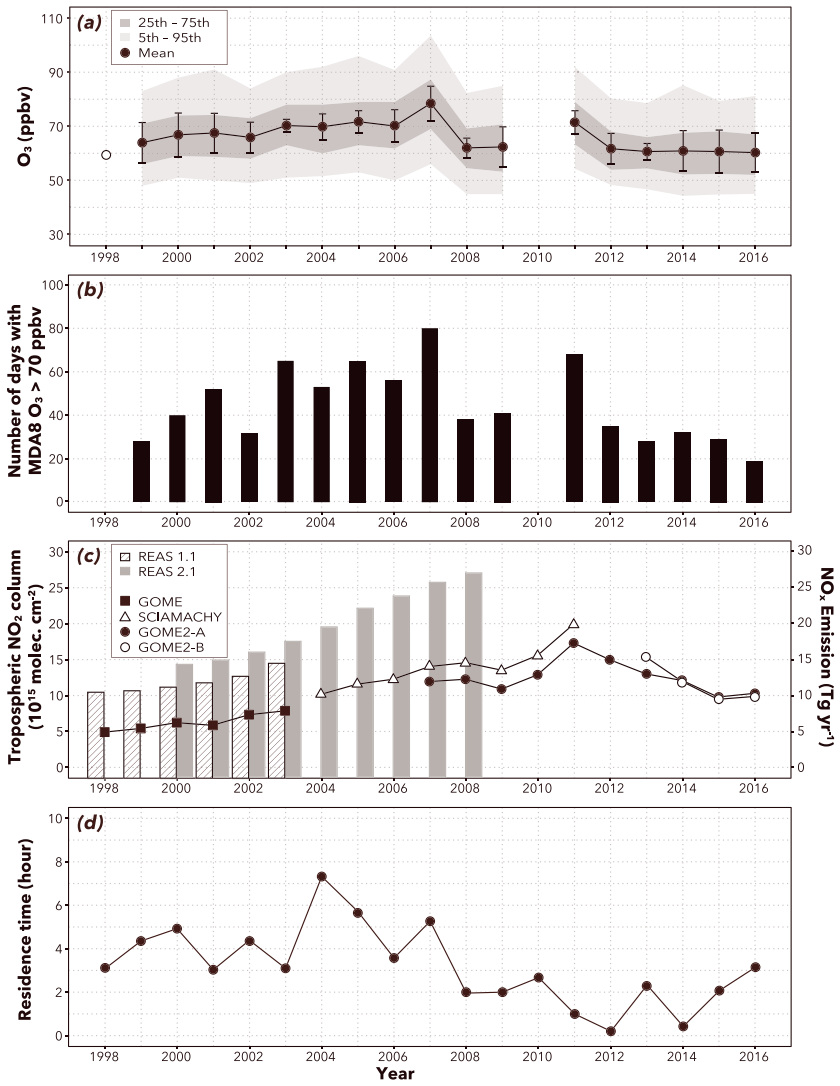

Figure 2. Time series of mean springtime tropospheric O_3 concentrations at Mt. Happo Observatory during 1998–2016. (a) The black filled circles with error bars indicate the seasonal mean ± the standard deviation, and the gray shading indicates percentile values. (b) The black bars indicate the number of days with maximum daily 8-hr average O_3 over 70 ppbv. (c) Satellite-derived tropospheric NO_2 column data are averaged over the central eastern China domain, and data on NO_x emissions from all of China are from REAS 1.1 (Ohara et al., 2007) and REAS 2.1 (Kurokawa et al., 2013). (d) Area-averaged residence times of air mass trajectories over the central eastern China domain.

Atmospheric Research (NCEP/NCAR) reanalysis data (2.5° × 2.5° grid) before 1997. All meteorological data are available from http://ready.arl.noaa.gov/archives.php/. The 5-day backward trajectory ensembles were initialized from a box, centered approximately at HPO and defined by 25 horizontal grid points (±0.125 and ±0.25°) and five altitude levels (±100 and ±200 m). A trajectory ensemble was calculated at 3-hr intervals beginning at 00:00 UTC (eight trajectory ensembles per day) for each day of the study period.

The analysis of the area-averaged residence time was made following previous studies (Naja et al., 2003; Pochanart, 2015; Pochanart et al., 2001). First, target domains were defined: one domain covered central eastern China (Figure 1; CEC; 30–40°N, 110–123°E) as the most polluted region, and another 1° × 1° grid domain covered the area around HPO. Second, for all trajectories, the residence times over the domains of all air masses that passed over the domains at an altitude below 3,000 m were averaged. To retain robust transport cases, the area-averaged residence times of CEC were calculated when at least 50% of the ensemble members passed over the CEC domain. Third, seasonal area-averaged residence times were calculated as the

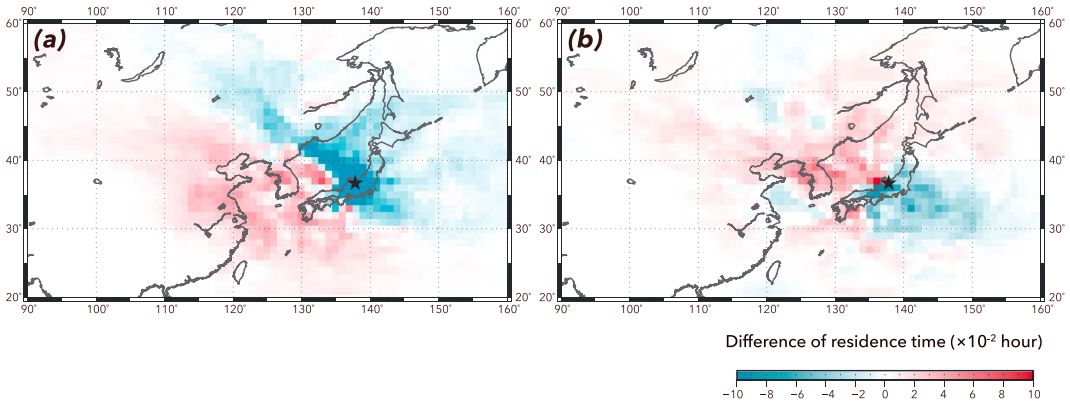

Figure 3. Distributions of differences in grid-averaged residence times. Differences are calculated as the values of (a) average residence times for 2004–2007 minus those for 2008–2013 and (b) average residence times for 1992–1996 minus those for 1999–2003. The black stars show the location of the Mt. Happo Observatory.

average of the averaged residence times from the trajectory ensembles of each season. We used the residence time as a measure of the atmospheric transport from source regions.

2.4. Meteorological Analysis

To examine the changes due to meteorological factors, we utilized sea level pressure (SLP), horizontal wind, and temperature data from the Japanese 55-year Reanalysis (JRA-55) data set, which is a global reanalysis data set constructed by the Japan Meteorological Agency (Harada et al., 2016; Kobayashi et al., 2015). There are two basic methods to quantify storm tracks. The first one identifies the extratropical storms, tracks their positions with time, and produces statistics for their distributions, while the other computes temporal band-pass-filtered eddy variance/covariance at a set of grid points with a retained frequency band highlighting the synoptic time scales (e.g., Guo et al., 2017). Eddy statistics such as the eddy momentum, heat, and moisture fluxes do not provide specific information regarding the storms, such as the intensity or frequency of occurrence. We employed meridional eddy heat transport at 850 hPa (v'T'850) to evaluate the storm track activity (Nakamura et al., 2002). The eddy components were obtained by applying a 10-day high-pass filter to the 6-hourly data set. For further details of the calculation, see Nakamura et al. (2002). In addition, we utilized sea surface temperature (SST) data compiled by the Hadley Centre (Rayner et al., 2003) and outgoing longwave radiation (OLR) observed by the satellite-based Advanced Very High Resolution Radiometer (AVHRR) (Liebmann & Smith, 1996). In the present analysis, the ENSO variability is represented by the Southern Oscillation Index (SOI; available at http://www.cpc.ncep.noaa.gov/data/indices/), while there are various ENSO indices. The SOI is defined as the observed SLP difference between Tahiti and Darwin (Trenberth, 1984). Positive and negative SOI values represent La Niña and El Niño episodes, respectively.

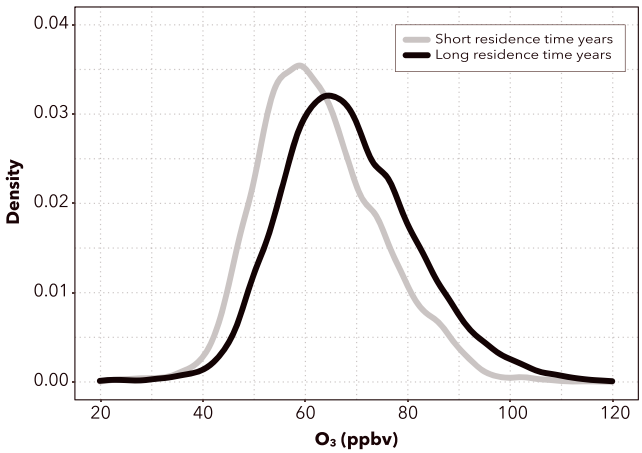

Figure 4. Distributions of hourly O_3 concentrations during short (2008–2015) and long (1999–2007 and 2016) area-averaged residence time years over the central eastern China domain. The threshold between short and long residence times was set to 3.5 h.

3. Results

3.1. Observed Trend of Springtime Ozone

During 1998–2006, the baseline level of springtime O_3 at HPO increased at a rate comparable to rates recorded at other northern midlatitude sites (0.3–0.8 ppbv/year), and the increase continued until 2007, when it peaked at 78 ppbv (Figure 2a). According to Tanimoto et al. (2009), changes in anthropogenic emissions and meteorology contributed almost equally to the observed O_3 growth at HPO during 1998–2003, but after 2003 the contribution of anthropogenic emissions became dominant. In 2008 and 2009, mean O_3 levels dropped to 62 ppbv. Such decrease can be seen in other seasons too (not shown). No measurements were obtained in 2010 because of instrument malfunction. In 2011, the O_3 level recovered to

Table 1
O_3 Concentrations (ppbv) During Short and Long Area-Averaged Residence Time Years Over CEC Domain

	Minimum	25th	Median	Mean	75th	Maximum
Long residence time years	6.0	59.2	67.0	68.5	77.0	143.9
Short residence time years	8.6	54.4	61.6	62.8	70.3	117.7

Note. The threshold between long and short residence times is 3.5 hr.

71 ppbv, but in 2012 it again dropped to 62 ppbv. From 2012 to 2016, O_3 levels were sustained at ~61 ppbv. Mean springtime O_3 levels before 2007 differed by as much as 10 ppbv from the levels after 2007. In addition, the O_3 variations were correlated with the number of days that the maximum daily 8-hr average (MDA8) O_3 exceeded 70 ppbv (Figure 2b). These data clearly indicate that the frequency of high-O_3 events controls the mean springtime O_3 levels.

From the 1990s through the 2000s, both tropospheric NO_2 columns over the CEC domain (Figure 1) and nationwide NO_x emissions in China show increasing trends (Figure 2c). Chinese nationwide NO_x emissions increased by approximately 150% during this period. Although the latest update to the inventory was made in 2008, satellite-derived tropospheric NO_2 column data show a peak in NO_x emissions in 2011, followed by a decreasing trend. This trend reversal in satellite-derived tropospheric NO_2 column data has been reported by other recent studies (Duncan et al., 2016; Irie et al., 2016; Krotkov et al., 2016). In 2011, the Chinese Government implemented its 12th Five-Year Plan (2011–2015), which aimed to reduce NO_x and sulfur dioxide (SO_2) emissions. Irie et al. (2016) suggested that the decreasing trend of tropospheric NO_2 vertical column density was caused by the widespread use of denitrification units in China; the installation of low-NO_x burners, especially in new power plants after 2005, and the implementation of new vehicle emission standards. Therefore, the O_3 decrease in 2012 and the subsequent low O_3 levels may have been influenced by decreased emissions of O_3 precursors from eastern China. However, the shift in springtime O_3 at HPO from an increasing trend to a decreasing trend occurred in 2007–2008, well before the emissions peak in 2011–2012.

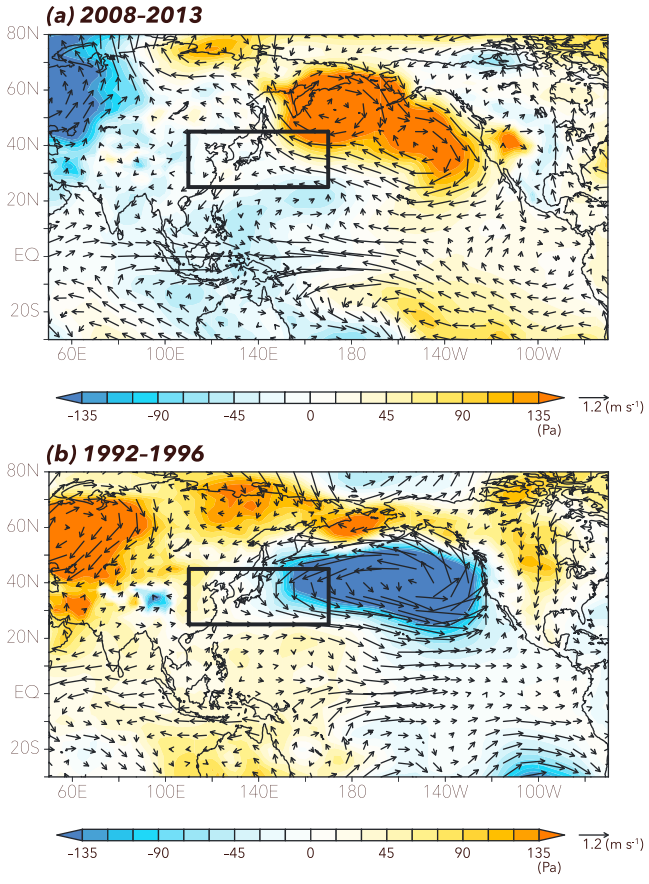

Figure 5. Anomalies of sea level pressure and wind vectors at 850 hPa for the periods (a) 2008–2013 and (b) 1992–1996. Anomalies were calculated relative to the climatology, defined as average values over the period from 1980 to 2016. The black rectangles show the region for averaging westerly wind anomaly in Figure 7a.

3.2. Changes in Residence Time

Figure 2d shows area-averaged residence times of air mass trajectories over CEC in spring calculated according to the method in previous studies (Naja et al., 2003; Pochanart, 2015; Pochanart et al., 2001). Residence times are a measure of temporal variations in the export of O_3 pollution from the CEC domain. Overall correlation of the residence time versus O_3 is not significant on the interannual (i.e., year-to-year) scale. Interestingly, the area-averaged residence time was higher during 2004–2007 than during other years, and it dropped to <5 hr in 2008. A possible explanation is that a meteorological shift in 2008 changed the impacts of long-range transport from the CEC domain and thus contributed to the decrease in O_3 concentrations at HPO. We confirmed that the 8.9 ppbv difference in the O_3 distributions between the two periods (2004–2007 and 2008–2013) was statistically significant ($p < 0.01$) by Wilcoxon rank sum test (Wilcoxon, 1945). The residence time difference between the high-O_3 (2004–2007) and low-O_3 (2008–2013) periods was positive over the CEC domain, the Korean Peninsula, the Yellow Sea, and the East China Sea, which are the most polluted domains in East Asia (Figure 3a), and was negative over north eastern China, far eastern Siberia, northern Japan, the Sea of Japan, and the North Pacific, which

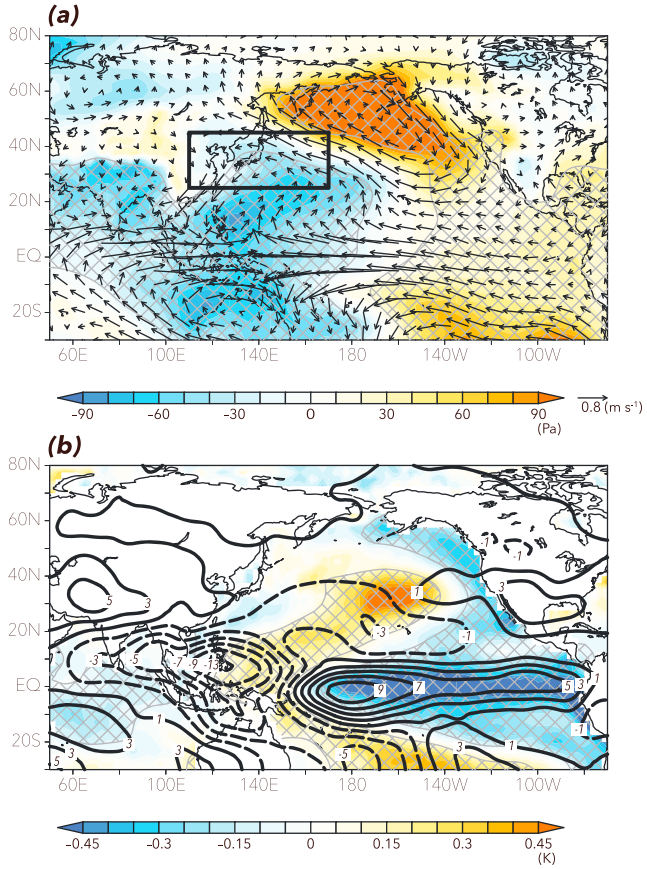

Figure 6. Regression maps of meteorological factors at 850 hPa with respect to the Southern Oscillation Index (SOI). (a) The color scale shows sea level pressure, and the vectors show wind speed anomalies. The hatching denotes areas in which the result of the regression of sea level pressure with respect to the SOI is significant at the 95% confidence level. (b) The color scale shows sea surface temperature, and the contours show outgoing longwave radiation (contour interval, 2 W/m^2), a measure of convective activity. The hatching denotes areas in which the result of the regression of SST with respect to the SOI is significant at the 95% confidence level.

are less polluted domains. HPO was obviously influenced by the polluted regions more strongly during the high-O_3 period than during the low-O_3 period. This result suggests that changes in the regional climate between these two periods induced changes in the long-range transport pathways of O_3 precursors, thereby causing changes in the O_3 levels at HPO.

We further investigated the frequency distributions of hourly O_3 concentrations at HPO between years with short (≤3.5 hr) and years with long (>3.5 hr) area-averaged residence times of air mass trajectories over the CEC domain (Figure 4 and Table 1). Residence times were long in 1999–2007 and 2016 and were short during other years. In both the highest and lowest concentration ranges, O_3 concentrations were obviously higher during long residence time years. In general, high springtime O_3 at HPO was associated with a long residence time over the CEC domain; Wilcoxon rank sum test (Wilcoxon, 1945) results confirmed that the difference in O_3 distributions between long and short residence time years was statistically significant ($p < 0.01$). Moreover, we estimated the difference between the two distributions to be 5.6 ppbv. These results indicate that the air mass trajectory residence time over the CEC domain is an important factor controlling the O_3 concentration at HPO.

3.3. Changes in Climate Pattern

The O_3 reduction during 2008–2013 despite increased NO_x emissions in China was likely due to a change in large-scale atmospheric circulation. Figure 5a shows SLP and horizontal wind anomalies for the period from 2008 to 2013 (relative to the climatology, defined as average values during 1980–2016 according to the JRA-55 data set). A low-pressure anomaly is evident over the south of Japan, and a high-pressure anomaly is located around the Aleutian Islands in the North Pacific. An anomalous geostrophic easterly wind between these pressure systems weakens air mass transport from East Asia (Figure 5a). Enhanced northerly winds in the west of Japan also contribute to a reduction in the transport of polluted air masses from East Asia to Japan. These results are consistent with the findings of Kurokawa et al. (2009), who showed that springtime surface O_3 levels in western and central Japan are higher than the climatological mean when the surface pressure anomaly over the North Pacific has a large negative value and are lower when the surface pressure anomaly has a positive value.

The circulation anomaly during 2008–2013 is reminiscent of the atmospheric response to ENSO, which is the dominant atmosphere-ocean coupled mode of climate variability over the tropical Pacific. We can clearly see high-pressure anomalies over the eastern Pacific and low-pressure anomalies over the western Pacific (Figure 5a). Figure 6a shows a regression map of SLP and horizontal wind with respect to the SOI during 1980–2016, indicating the distributions of expected SLP and horizontal wind anomalies in La Niña years (SOI = 1). The horizontal pattern of the SLP anomaly (Figure 5a) resembles the SLP regression results (Figure 6a; pattern correlation, 0.84), suggesting that La Niña-like wind persisted during 2008–2013. Figure 6b also indicates the distributions of expected SST and OLR anomalies in La Niña years (SOI = 1). In La Niña years, SST is warmer in the western part of the equatorial Pacific and cooler in the central to eastern parts (Figure 6b). The warm SST anomaly in the western Pacific extends northeastward and southeastward, producing a horseshoe-shaped pattern. Convective activity is enhanced, and low-pressure anomalies are evident over regions with warmer SSTs. Meanwhile, the Rossby wave response to the tropical forcing results in high-pressure anomalies around the Aleutian Islands over the North Pacific (Jin & Hoskins, 1995).

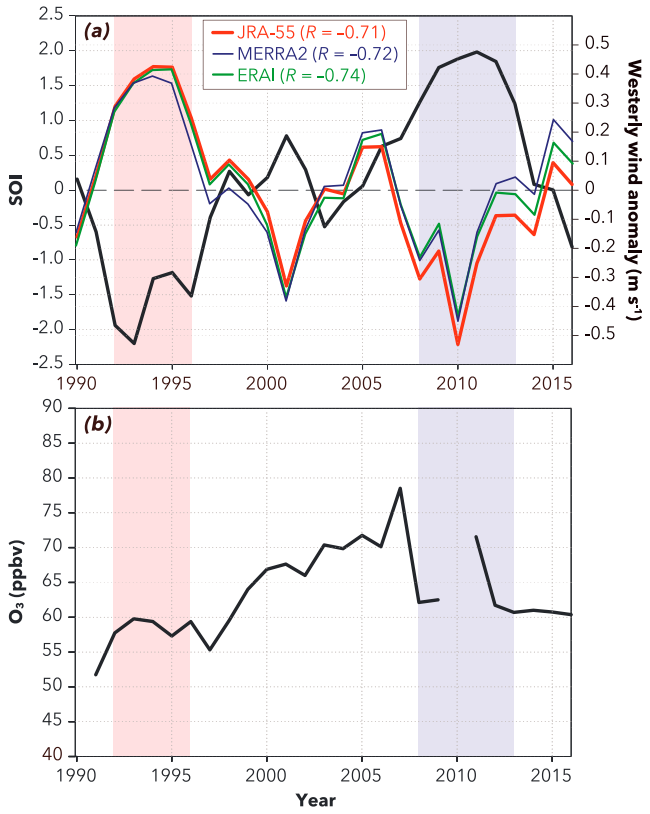

Figure 7. Time series of the Southern Oscillation Index (SOI), westerly wind anomalies, and springtime O_3 concentrations at Mt. Happo Observatory. (a) Time series of the normalized SOI (black) and westerly wind anomalies from Japanese 55-year Reanalysis (JRA-55; red), Modern-Era Retrospective analysis for Research and Applications, Version 2 (MERRA2; blue), and European Centre for Medium-Range Weather Forecasts Interim Re-Analysis (ERAI; green) around Japan (25–45°N, 110–170°E), smoothed by using 5-year running means. (b) Time series of springtime O_3 concentrations at Mt. Happo Observatory from 1992 to 2016 (Tanimoto, 2009). The blue and red shades indicate the La Niña and El Niño-like wind pattern years, respectively.

Figure 7a shows time series of the normalized SOI and zonal wind anomaly around Japan (25–45°N, 110–170°E; black rectangle area in Figure 5). Here the zonal wind anomaly represents the strength of the anomalous circulation around Japan. To focus on the long-term variability, we applied 5-year running means to the following time series analysis. The results without the running means were qualitatively similar but not significant, possibly due to year-to-year meteorological variability (not shown).

A positive and negative SOI corresponds to La Niña-like and El Niño-like conditions, respectively. The correlation coefficient between the SOI and the zonal wind anomaly was −0.71 ($p < 0.01$). To support the robustness of the relationship between SOI and zonal wind anomaly around Japan, we compared the results using JRA-55 with those using the Modern-Era Retrospective analysis for Research and Applications, Version 2 (MERRA2; Bosilovich et al., 2015) and the European Centre for Medium-Range Weather Forecasts Interim Re-Analysis (ERAI; Dee et al., 2011). The significant relationship between the anomalous westerlies and SOI are robust in all the data sets (Figure 7a). The correlation coefficient between the SOI and the zonal wind anomaly in MERRA2 and ERAI was −0.72 and −0.74, respectively. In La Niña years, mean westerly wind anomaly around Japan (black rectangle area in Figure 6a) is expected to be −0.22 m/s. The years from 2008 to 2013 were high SOI years (SOI = 1.66), and they were associated with a negative westerly wind anomaly (−0.33 m/s). It means that the negative westerly wind anomaly during 2008–2013 was associated with the La Niña-like condition. This period also corresponds to the period of O_3 suppression at HPO (Figure 7b). If this La Niña-like wind pattern had not occurred and continued, the O_3 trend at HPO would have continued upward, and the mean springtime O_3 level might have exceeded 70 ppbv by the early 2010s like in China and South Korea (Ma et al., 2016; Shin et al., 2017).

In addition, the O_3 time series shows a rounded peak (an enhancement of ~5 ppbv) during 1992–1996 (Figure 7b), corresponding to a period of negative SOI and enhanced westerly winds (Figure 7a). The high-pressure anomalies over the western Pacific and the low-pressure anomalies around the Aleutian Islands in the North Pacific during this period represent the typical atmospheric response to El Niño (Figure 5b). A small drop in O_3 of approximately 4 ppbv observed at HPO in 1996–1997, before the large O_3 increase that began in 1998, corresponded to weakened westerly winds. The geographical distribution of the difference in the grid-averaged residence time between the low-SOI (1992–1996) and high-SOI (1999–2003) periods shows that residence times over the region west of Japan increased and those over the Pacific Ocean decreased (Figure 3b). These results suggest that the persistent El Niño-like wind pattern during 1992–1996 led to enhanced O_3 concentrations at HPO via meteorological conditions that favored the transport of polluted air masses from East Asia to the western Pacific. If this El Niño-like wind pattern had not occurred, the O_3 at HPO would have been lower during 1992–1996 and would show a monotonic increase from 1991 to 2007, corresponding to the monotonic increase in NO_x emissions over China (~220%) from the 1990s to 2000s in REAS 1.1 (Ohara et al., 2007).

3.4. Multiple Regression Analysis

Finally, we performed a multiple regression analysis to quantify the importance of the atmospheric transport relative to the increase of the Chinese emissions for the O_3 variability. We combined the two NO_x emission and four tropospheric NO_2 column data sets (Figure 2c) to obtain a single time series by adjusting the average and the standard deviation of each data set, assuming that the regional mean of satellite-derived tropospheric NO_2 column reflects the surface emissions. For example, REAS 1.1 and 2.1 were

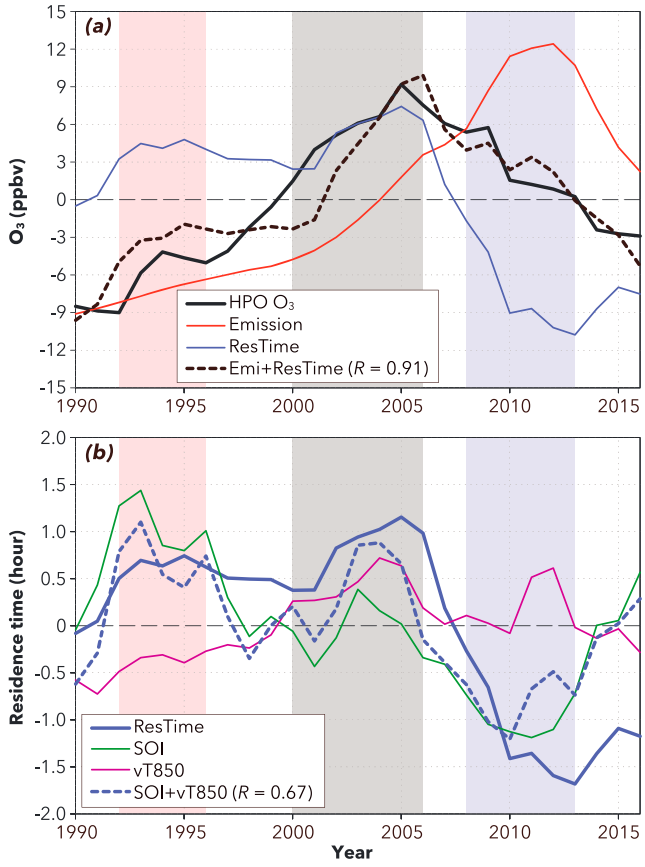

Figure 8. Multiple regression of the decadal O_3 changes at Mt. Happo Observatory (HPO). (a) The multiple regression of the O_3 changes at HPO (1990–2016 average was removed and smoothed by 5-year running means) with respect to the combined emissions (red) and the residence time (blue). (b) Multiple regression of the residence time with respect to the Southern Oscillation Index (SOI; green) and v'T'850 (violet) averaged around Japan (25–45°N, 110–170°E). The blue and red shades indicate the La Niña and El Niño-like wind pattern years, respectively. The gray shade indicates the enhanced storm track activity years.

available for 1980–2003 and 2000–2008, respectively, and the combined emissions of these two data sets were calculated as

$$\text{combined emissions} = \begin{cases} \text{REAS1.1}_{80-99} \\ \left(\text{REAS1.1}_{00-03} + \text{REAS2.1}^{\text{adj}}_{00-03}\right)/2 \\ \text{REAS2.1}^{\text{adj}}_{04-08} \end{cases}$$

$$\text{REAS2.1}^{\text{adj}}_{00-08} = (\text{REAS2.1}_{00-08} - \text{REAS2.1}^{\text{avr}}) \times \frac{\text{REAS1.1}^{\text{std}}}{\text{REAS2.1}^{\text{std}}} + \text{REAS1.1}^{\text{avr}}$$

where subscripts indicated the period, adj was the adjusted value, and avr and std were the average and the standard deviation for the overlapping years of 2000–2003. Similarly, NO_x emission and tropospheric NO_2 column data sets were adjusted, and then a single time series of emissions was obtained (red line in Figure 8a). We confirmed that the following results were not sensitive to the details of the combining method.

Based on a multiple regression analysis, the O_3 variability was expressed by the time series of the combined emissions and the residence time ($O_3 \approx \alpha$ Emission + β ResTime; α and β are the regression coefficients) using the least squares method as shown in Figure 8a. The correlation coefficient of the O_3 and α Emission + β ResTime was 0.91, meaning that the O_3 variability was mostly determined by the emissions and the atmospheric transport represented by the residence time. The O_3 increase from 1990 to 2005 basically reflected the emission increase (α Emission), whereas the decrease after 2005 was largely explained by the residence time (β ResTime). In addition, the residence time showed some contribution to the O_3 increase around 2005.

We further examined the residence time by a multiple regression analysis with respect to the SOI and the v'T'850 averaged around Japan (ResTime ≈ γ SOI + δ v'T'850; γ and δ are the regression coefficients) as shown in Figure 8b. The effects of the SOI increased the residence time during 1992–1996 and decreased it during 2008–2013, which is consistent with the results described above. On the other hand, the large positive value of the residence time during 2000–2006 corresponds to the enhanced v'T'850. Although we did not look into the detailed meteorological mechanisms of the variations in the storm track activities around Japan, this strongly suggests the importance of the storm track activities in controlling the changes in O_3 at HPO, consistent with a previous analysis that midlatitude storms play a role in redistributing O_3 over the North Pacific (e.g., Knowland et al., 2015). Figure 9 shows anomalies of v'T'850, SLP, and horizontal wind during 2000–2006. The positive v'T'850 around Japan indicates the enhanced storm track activities. The negative anomalies of SLP to the west of Japan accompanied by the westerly wind anomalies suggest an increased outflow from East Asia.

4. Discussion

To evaluate the robustness of the analysis at HPO, a single mountain site, we further examined the O_3 time series observed at surface observatories located in western and central Japan and applied the multiple regression analysis. In Japan, continuous measurements of O_3 at ground level are conducted throughout the country. The observatories are managed and operated by the Ministry of the Environment (MOE) of Japan and by local governments. The monitoring data were compiled by the Atmospheric Environmental Regional Observation System (AEROS). The AEROS data are available from https://www.nies.go.jp/igreen/. For calculation of the mean springtime O_3 in western and central Japan (WCJ O_3),

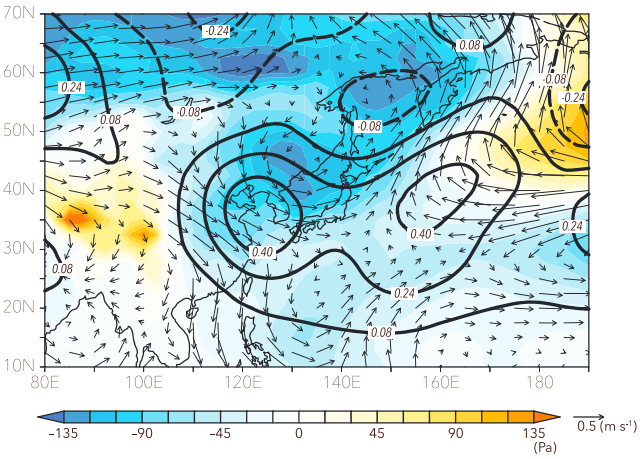

Figure 9. Anomalies of v′T′ and wind vectors at 850 hPa, and sea level pressure for the periods 2000–2006. Anomalies were calculated relative to the climatology, defined as average values over the period from 1980 to 2016. The color scale shows sea level pressure anomaly, vectors show wind anomaly, and contours show v′T′ anomaly (contour interval, 0.16 K m/s), a measure of storm track activity.

we used daytime O_3 data (between 09:00 and 15:00 JST) in the south of 37°N, which is almost the same region as that in Kurokawa et al. (2009). In contrast to HPO, the average altitude of these observatories is approximately 50 m.

In Figure 10a, the average WCJ O_3 shows an increasing trend since the early-1990s through the late-2000s, followed by a slight decrease in 2010 and flattening until 2016. This long-term trend was consistent with that at HPO, suggesting that the nonincreasing feature in the late-2000s and early-2010s was a regional phenomenon. From the multiple regression analysis, the correlation coefficient of the average WCJ O_3 and α Emission + β ResTime was 0.92, the same as that for HPO. The multiple regression of the average WCJ O_3 indicated that the WCJ O_3 increased with the increasing emissions in the 1990s and 2000s and decreased with the decreasing residence time after 2005, despite increasing Chinese emissions. It should be also noted that the WCJ O_3 had a small increase in 1992–1996 (with a peak in 1995) and a decrease in 2008–2013, which happened prior to the decrease of Chinese emissions.

The influence of the decadal wind shifts associated with the El Niño and La Niña-like climate to O_3 can be seen more clearly at a remote marine boundary layer site, Minamitorishima (MNM, 24.28°N, 153.98°E, 8 m above sea level; Figure 1) in the North Pacific. MNM is one of the Global Atmosphere Watch (GAW) Global stations operated by the Japan Meteorological Agency and is located on a small island (~1.4 km^2) at a distance of approximately 3,500 km from the continent. It was reported that MNM was affected by Asian emissions, especially, in spring (Wada et al., 2013). The O_3 data at MNM are provided by the GAW World Data Centre for Reactive Gases (WDCRG; https://www.gaw-wdcrg.org/). In contrast to HPO and WCJ, the long-term record of surface O_3 at MNM shows no obvious increasing trend, but distinct interannual variations over the past decades (thick solid black line in Figure 10b). Here we also examined the MNM O_3 time series by a multiple regression analysis and found reasonably good results with the emission and the SOI ($O_3 \approx \varepsilon$ Emission + ζ SOI; ε and ζ are the regression coefficients). The correlation coefficient of the MNM O_3 and ε Emission + ζ SOI was 0.83. We can see that the variations of the MNM O_3 were closely linked to those of the SOI. In particular, we see a positive O_3 anomaly in 1992–1996 and a negative O_3 anomaly in 2008–2013. It is also interesting to note that the O_3 decrease in 2008–2013 was suppressed in the latter half of this period, likely due to the contribution of the Chinese emissions, which peaked in 2011–2013. These results indicate that the O_3 variability at MNM was mainly controlled by the atmospheric transport, with small contributions from the Chinese emissions.

For remote marine sites such as MNM and MLO (Lin et al., 2014), which are located far from heavily polluted source regions in East Asia, the relative impacts of the changes in long-range transport are greater than those of the changes in emissions for the springtime O_3 variability. The changes are controlled mainly by the transport associated with SOI, as the O_3 variations at MNM are reconciled by the multiple regression of the changes in the Asian emissions and the SOI, with the SOI being more important. For the sites near the continent, such as HPO and WCJ, the impacts of the changes both in long-range transport and in emissions are important in shaping the long-term trend of springtime O_3. The 25-year trends of O_3 at HPO and WCJ were substantially modulated by the changes in transport. The controlling factors of the long-range transport at HPO and WCJ were more complicated than those at MNM and MLO. Not only subdecadal variability but also synoptic-scale variability in storm track activities in the Asian Pacific rim region is equally important. In the present work, we show for the first time that the impacts of the decadal wind shifts associated with SOI are not limited to the subtropical island sites in the Pacific Ocean, but, rather, they are great enough to perturb the decadal changes and long-term trends of lower tropospheric O_3 in the northern midlatitudes in the East Asian Pacific rim region, which has been associated with a rapid increase in anthropogenic emissions over the past decades. An important implication is that in addition to the reduction of emissions, atmospheric circulation changes on different temporal (i.e., weeks to years) and spatial (i.e., 100 to 1,000 km) scales need to be considered in targeting improved

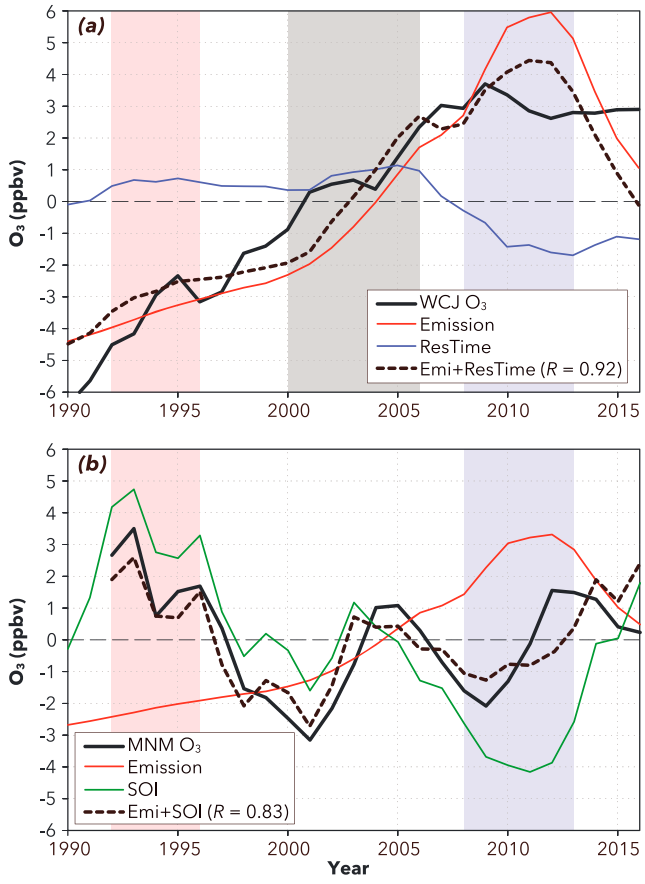

Figure 10. The multiple regressions of the decadal O_3 changes in western and central Japan (WCJ) and at Minamitorishima (MNM). (a) The multiple regression of the O_3 changes in WCJ (1990–2016 average was removed and smoothed by 5-year running means) with respect to the combined emissions (red) and the residence time (blue). (b) The multiple regression of the O_3 changes at MNM (1994–2016 average was removed and smoothed by 5-year running means) with respect to the combined emissions (red) and the SOI (green). The blue and red shades indicate the La Niña and El Niño-like wind pattern years, respectively. The gray shade indicates the enhanced storm track activity years.

air quality in East Asia, where the health impacts of air pollution are now one of the top environmental concerns. It becomes increasingly important to consider such climatic factors, because future climate changes including ENSO, monsoon circulation, and storm track are projected during the 21st century (Intergovernmental Panel on Climate Change, 2013).

Emissions of NMVOCs from anthropogenic and biogenic sources should also be considered because those are important O_3 precursors. The anthropogenic emissions of NMVOCs in China are estimated at 22.1 and 23.6 Tg for 2008 and 2010, respectively, and they increased by 14% during 2006–2010 in the MIX inventory (Li et al., 2017). Changes in the emissions of biogenic volatile organic compounds (BVOCs) are influenced by changes in climate conditions as well as changes in land cover and land use. Fu and Liao (2014) estimated the changes in BVOCs emissions in China from the late 1980s to the mid-2000s by using the global chemical transport model and the land cover data set derived from remote sensing images and land use surveys. They estimated the total emissions of BVOCs in China at 16.8 Tg in the mid-2000s, which is an increase of 11.4% relative to the late 1980s, due to the combined effect of meteorology and land cover. A significant increase in the emissions of isoprene (>10%), the dominant BVOCs emitted in present-climate state (Guenther et al., 2012), was found in central China during 2000–2015 with a large increase in tree coverage (~13%) because of extensive afforestation efforts (Chen et al., 2018). These results suggest that emissions of NMVOCs from China did not decrease after 2008. In addition, Jin et al. (2017) showed that surface O_3 production in spring is mostly sensitive to NO_x over western and central Japan, based on the space-based tropospheric column ratio of formaldehyde to NO_2. Therefore, we believe that the decrease of O_3 after 2008 is not due to the changes in emissions of NMVOCs.

Vegetation can modulate tropospheric O_3 burden via dry deposition as well as BVOC emissions. Dry deposition of O_3 is a dominant physical loss process and accounts for approximately 20% of annual global tropospheric O_3 loss (e.g., Young et al., 2018). In typical chemical transport models, dry deposition is parameterized as a function of surface type and atmospheric stability conditions due to the vast environmental complexities (Wesely & Hicks, 2000). Fu and Tai (2015) showed that springtime O_3 concentration was increased in the range of 0.5–2 ppbv for the period 1980–2010 in most of China largely due to the decrease of dry deposition velocity driven by land cover and land use change alone. This increase is small compared to the changes in the springtime O_3 at HPO. Therefore, we believe that the decrease of O_3 after 2008 is not due to the changes in dry deposition.

5. Conclusions

In this study, we analyzed the springtime O_3 trend and its controlling factors at a high-altitude site in Japan from 1998 to 2016. The mean springtime O_3 had increased until 2007 and was correlated with the increase of NO_x emissions from China. In 2008, the O_3 levels dropped to 62 ppbv even though Chinese emissions still increased. In 2011, the mean O_3 level recovered to 71 ppbv, but in 2012 it again dropped to 62 ppbv. From 2012 to 2016, the O_3 levels were sustained at ~61 ppbv. Based on the analysis of transport pattern and associated meteorology, we showed that persistent La Niña-like wind pattern from 2008 to 2013 suppressed the long-range transport from East Asia via weakened westerly winds. On the contrary, the El Niño-like wind pattern from 1992 to 1996 favored long-range transport from East Asia via strengthened westerly winds. In addition, the enhanced storm track activities from 2000 to 2006 also contributed to the

enhancement of long-range transport from East Asia. These results indicate that the persistent La Niña-like wind pattern led to reduced O_3 concentrations at HPO and that the persistent El Niño-like climate and the enhanced storm track activities led to the enhanced O_3 concentrations. For the sites near the continent, such as HPO and WCJ, the impacts of both the changes in long-range transport and in emissions are important in shaping the long-term trend of springtime O_3. For remote marine sites such as MNM, the relative impacts of the changes in long-range transport are greater than those of the changes in emissions for the springtime O_3 variability.

In conclusion, this study revealed, based on observational data for the first time, that the variations of La Niña- and El Niño-like wind patterns affect the long-range transport of pollutants from East Asia and thus the decadal changes and long-term trends of O_3 in the lower free troposphere in East Asia and the North Pacific. Without this climatic effect, the O_3 trend over Japan as well as at HPO would have been further upward in the late 2000s and early 2010s.

Acknowledgments

We acknowledge the free use of tropospheric NO_2 column data from the GOME, SCIAMACHY, and GOME-2 sensors from the Tropospheric Emission Monitoring Internet Service (TEMIS http://www.temis.nl/), O_3 data at Mt. Happo provided by the Acid Deposition Monitoring Network in East Asia (EANET; http://www.eanet.asia/product/), O_3 data at Minamitorishima provided by the GAW World Data Centre for Reactive Gases (WDCRG; https://www.gaw-wdcrg.org/), O_3 data in western and central Japan provided by the National Institute for Environmental Studies (NIES; https://www.nies.go.jp/igreen/), the global Japanese 55-year Reanalysis (JRA-55) data set from the Japan Meteorological Agency, and interpolated outgoing longwave radiation data provided by the NOAA/OAR/ESRL Physical Science Division (https:www.esrl.noaa.gov/psd/). We also acknowledge the staff members of the Asia Center for Air Pollution Research, the Nagano Environmental Conservation Research Institute, and the Ministry of the Environment, Japan (MOE), for carrying out the O_3 measurements. Furthermore, we thank Hideki Nara and Shigeru Hashimoto from the National Institute for Environmental Studies for their valuable comments and technical help. Financial support was provided by the Environmental Research and Technology Development Fund (2-1505 and 2-1803) of MOE and the Environmental Restoration and Conservation Agency, the Global Environment Research Account for National Institutes of MOE, and Coordination Funds for Promoting AeroSpace Utilization of the Ministry of Education, Culture, Sports, Science and Technology, Japan.

References

Acid Deposition Monitoring Network in East Asia (2013). *Technical manual for air concentration monitoring in East Asia*. Niigata: Network Center for EANET.

Boersma, K. F., Eskes, H. J., & Brinksma, E. J. (2004). Error analysis for tropospheric NO_2 retrieval from space. *Journal of Geophysical Research*, *109*, D04311. https://doi.org/10.1029/2003JD003962

Bosilovich, M. G., Akella, S., Coy, L., Cullather, R., Draper, C., Gelaro, R., et al. (2015). MERRA-2: Initial evaluation of the climate. In R. D. Koster (Ed.), *Technical report series on global modeling and data assimilation* (Vol. 43, 139 pp.). Greenbelt, MD: Goddard Space Flight Center.

Chang, K.-L., Petropavlovskikh, I., Cooper, O. R., Schultz, M. G., & Wang, T. (2017). Regional trend analysis of surface ozone observations from monitoring networks in eastern North America, Europe and East Asia. *Elementa: Science of the Anthropocene*, *5*, 50. https://doi.org/10.1525/elementa.243

Chen, W. H., Guenther, A. B., Wang, X. M., Chen, Y. H., Gu, D. S., Chang, M., et al. (2018). Regional to global biogenic isoprene emission responses to changes in vegetation from 2000 to 2015. *Journal of Geophysical Research: Atmospheres*, *123*, 3757–3771. https://doi.org/10.1002/2017JD027934

Cooper, O. R., Parrish, D. D., Stohl, A., Trainer, M., Nédélec, P., Thouret, V., et al. (2010). Increasing springtime ozone mixing ratios in the free troposphere over western North America. *Nature*, *463*(7279), 344–348. https://doi.org/10.1038/nature08708

Cuevas, E., González, Y., Rodríguez, S., Guerra, J. C., Gómez-Peláez, A. J., Alonso-Pérez, S., et al. (2013). Assessment of atmospheric processes driving ozone variations in the subtropical North Atlantic free troposphere. *Atmospheric Chemistry and Physics*, *13*(4), 1973–1998. https://doi.org/10.5194/acp-13-1973-2013

Dee, D. P., Uppala, S. M., Simmons, A. J., Berrisford, P., Poli, P., Kobayashi, S., et al. (2011). The ERA-Interim reanalysis: Configuration and performance of the data assimilation system. *Quarterly Journal of the Royal Meteorological Society*, *137*(656), 553–597. https://doi.org/10.1002/qj.828

Dentener, F., Keating, T., & Akimoto, H. (Eds.) (2010). *Hemispheric transport of air pollution 2010. Part A: Ozone and particulate matter (Air Pollution Studies No. 17)*. New York and Geneva: United Nations.

Draxler, R. R. (1999). *HYSPLIT4 user's guide (NOAA Tech. Memo. ERL ARL-230)*. Silver Spring, MD: NOAA Air Resources Laboratory.

Draxler, R. R., & Hess, G. D. (1997). *Description of the HYSPLIT_4 modeling system (NOAA Tech. Memo. ERL ARL-224)*. Silver Spring, MD: NOAA Air Resources Laboratory.

Draxler, R. R., & Hess, G. D. (1998). An overview of the HYSPLIT_4 modelling system for trajectories. *Australian Meteorological Magazine*, *47*, 295–308.

Duncan, B. N., Lamsal, L. N., Thompson, A. M., Yoshida, Y., Lu, Z., Streets, D. G., et al. (2016). A space-based, high-resolution view of notable changes in urban NOx pollution around the world (2005–2014). *Journal of Geophysical Research: Atmospheres*, *121*, 976–996. https://doi.org/10.1002/2015jd024121

Fiore, A. M., Naik, V., & Leibensperger, E. M. (2015). Air quality and climate connections. *Journal of the Air & Waste Management Association (1995)*, *65*(6), 645–685. https://doi.org/10.1080/10962247.2015.1040526

Fu, Y., & Liao, H. (2014). Impacts of land use and land cover changes on biogenic emissions of volatile organic compounds in China from the late 1980s to the mid-2000s: Implications for tropospheric ozone and secondary organic aerosol. *Tellus B*, *66*(1), 24987. https://doi.org/10.3402/tellusb.v66.24987

Fu, Y., & Tai, A. P. K. (2015). Impact of climate and land cover changes on tropospheric ozone air quality and public health in East Asia between 1980 and 2010. *Atmospheric Chemistry and Physics*, *15*(17), 10,093–10,106. https://doi.org/10.5194/acp-15-10093-2015

Gaudel, A., Cooper, O. R., Ancellet, G., Barret, B., Boynard, A., Burrows, J. P., et al. (2018). Tropospheric ozone assessment report: Present-day distribution and trends of tropospheric ozone relevant to climate and global atmospheric chemistry model evaluation. *Elementa: Science of the Anthropocene*, *6*(1), 39. https://doi.org/10.1525/elementa.291

Guenther, A. B., Jiang, X., Heald, C. L., Sakulyanontvittaya, T., Duhl, T., Emmons, L. K., & Wang, X. (2012). The Model of Emissions of Gases and Aerosols from Nature version 2.1 (MEGAN2.1): An extended and updated framework for modeling biogenic emissions. *Geoscientific Model Development*, *5*(6), 1471–1492. https://doi.org/10.5194/gmd-5-1471-2012

Guo, Y., Shinoda, T., Lin, J., & Chang, E. K. M. (2017). Variations of Northern Hemisphere storm track and extratropical cyclone activity associated with the Madden–Julian Oscillation. *Journal of Climate*, *30*(13), 4799–4818. https://doi.org/10.1175/JCLI-D-16-0513.1

Harada, Y., Kamahori, H., Kobayashi, C., Endo, H., Kobayashi, S., Ota, Y., et al. (2016). The JRA-55 reanalysis: Representation of atmospheric circulation and climate variability. *Journal of the Meteorological Society of Japan*, *94*(3), 269–302. https://doi.org/10.2151/jmsj.2016-015

Intergovernmental Panel on Climate Change (2013). Climate change 2013: The physical science basis. In *Contribution of Working Group I to the Fifth Assessment Report of the Intergovernmental Panel on Climate Change* (1535 pp.). Cambridge, UK and New York: Cambridge University Press.

Irie, H., Muto, T., Itahashi, S., Kurokawa, J. -I., & Uno, I. (2016). Turnaround of tropospheric nitrogen dioxide pollution trends in China, Japan, and South Korea. *SOLA*, *12*(0), 170–174. https://doi.org/10.2151/sola.2016-035

Jin, F., & Hoskins, B. J. (1995). The direct response to tropical heating in a baroclinic atmosphere. *Journal of the Atmospheric Sciences*, *52*(3), 307–319. https://doi.org/10.1175/1520-0469(1995)052<0307:TDRTTH>2.0.co;2

Jin, X., Fiore, A. M., Murray, L. T., Valin, L. C., Lamsal, L. N., Duncan, B., et al. (2017). Evaluating a space-based indicator of surface ozone-NO_x-VOC sensitivity over midlatitude source regions and application to decadal trends. *Journal of Geophysical Research: Atmospheres*, *122*, 10,439–10,461. https://doi.org/10.1002/2017JD026720

Kato, S., Pochanart, P., Hirokawa, J., Kajii, Y., Akimoto, H., Ozaki, Y., et al. (2002). The influence of Siberian forest fires on carbon monoxide concentrations at Happo, Japan. *Atmospheric Environment*, *36*(2), 385–390. https://doi.org/10.1016/s1352-2310(01)00158-3

Knowland, K. E., Doherty, R. M., & Hodges, K. I. (2015). The effects of springtime mid-latitude storms on trace gas composition determined from the MACC reanalysis. *Atmospheric Chemistry and Physics*, *15*(6), 3605–3628. https://doi.org/10.5194/acp-15-3605-2015

Knowland, K. E., Doherty, R. M., Hodges, K. I., & Ott, L. E. (2017). The influence of mid-latitude cyclones on European background surface ozone. *Atmospheric Chemistry and Physics*, *17*(20), 12,421–12,447. https://doi.org/10.5194/acp-17-12421-2017

Kobayashi, S., Ota, Y., Harada, Y., Ebita, A., Moriya, M., Onoda, H., et al. (2015). The JRA-55 Reanalysis: General specifications and basic characteristics. *Journal of the Meteorological Society of Japan*, *93*(1), 5–48. https://doi.org/10.2151/jmsj.2015-001

Krotkov, N. A., McLinden, C. A., Li, C., Lamsal, L. N., Celarier, E. A., Marchenko, S. V., et al. (2016). Aura OMI observations of regional SO_2 and NO_2 pollution changes from 2005 to 2015. *Atmospheric Chemistry and Physics*, *16*(7), 4605–4629. https://doi.org/10.5194/acp-16-4605-2016

Kurokawa, J. -I., Ohara, T., Morikawa, T., Hanayama, S., Janssens-Maenhout, G., Fukui, T., et al. (2013). Emissions of air pollutants and greenhouse gases over Asian regions during 2000–2008: Regional Emission inventory in ASia (REAS) version 2. *Atmospheric Chemistry and Physics*, *13*(21), 11,019–11,058. https://doi.org/10.5194/acp-13-11019-2013

Kurokawa, J. -I., Ohara, T., Uno, I., Hayasaki, M., & Tanimoto, H. (2009). Influence of meteorological variability on interannual variations of springtime boundary layer ozone over Japan during 1981–2005. *Atmospheric Chemistry and Physics*, *9*(17), 6287–6304. https://doi.org/10.5194/acp-9-6287-2009

Leibensperger, E. M., Mickley, L. J., & Jacob, D. J. (2008). Sensitivity of US air quality to mid-latitude cyclone frequency and implications of 1980–2006 climate change. *Atmospheric Chemistry and Physics*, *8*(23), 7075–7086. https://doi.org/10.5194/acp-8-7075-2008

Li, M., Zhang, Q., Kurokawa, J.-I., Woo, J.-H., He, K., Lu, Z., et al. (2017). MIX: A mosaic Asian anthropogenic emission inventory under the international collaboration framework of the MICS-Asia and HTAP. *Atmospheric Chemistry and Physics*, *17*(2), 935–963. https://doi.org/10.5194/acp-17-935-2017

Liebmann, B., & Smith, C. A. (1996). Description of a complete (interpolated) outgoing longwave radiation dataset. *Bulletin of the American Meteorological Society*, *77*(6), 1275–1277.

Lin, M., Fiore, A. M., Horowitz, L. W., Langford, A. O., Oltmans, S. J., Tarasick, D., & Rieder, H. E. (2015). Climate variability modulates western US ozone air quality in spring via deep stratospheric intrusions. *Nature Communications*, *6*(1), 7105. https://doi.org/10.1038/ncomms8105

Lin, M., Horowitz, L. W., Oltmans, S. J., Fiore, A. M., & Fan, S. (2014). Tropospheric ozone trends at Mauna Loa Observatory tied to decadal climate variability. *Nature Geoscience*, *7*(2), 136–143. https://doi.org/10.1038/ngeo2066

Liu, X., Kondo, Y., Ram, K., Matsui, H., Nakagomi, K., Ikeda, T., et al. (2013). Seasonal variations of black carbon observed at the remote mountain site Happo in Japan. *Journal of Geophysical Research: Atmospheres*, *118*, 3709–3722. https://doi.org/10.1002/jgrd.50317

Ma, Z., Xu, J., Quan, W., Zhang, Z., Lin, W., & Xu, X. (2016). Significant increase of surface ozone at a rural site, north of eastern China. *Atmospheric Chemistry and Physics*, *16*(6), 3969–3977. https://doi.org/10.5194/acp-16-3969-2016

Miyazaki, K., Eskes, H., Sudo, K., Boersma, K. F., Bowman, K., & Kanaya, Y. (2017). Decadal changes in global surface NOx emissions from multi-constituent satellite data assimilation. *Atmospheric Chemistry and Physics*, *17*(2), 807–837. https://doi.org/10.5194/acp-17-807-2017

Monks, P. S., Granier, C., Fuzzi, S., Stohl, A., Williams, M. L., Akimoto, H., et al. (2009). Atmospheric composition change—Global and regional air quality. *Atmospheric Environment*, *43*(33), 5268–5350. https://doi.org/10.1016/j.atmosenv.2009.08.021

Naja, M., Akimoto, H., & Staehelin, J. (2003). Ozone in background and photochemically aged air over central Europe: Analysis of long-term ozonesonde data from Hohenpeissenberg and Payerne. *Journal of Geophysical Research*, *108*(D2), 4063. https://doi.org/10.1029/2002JD002477

Nakamura, H., Izumi, T., & Sampe, T. (2002). Interannual and decadal modulations recently observed in the Pacific storm track activity and East Asian winter monsoon. *Journal of Climate*, *15*(14), 1855–1874. https://doi.org/10.1175/1520-0442(2002)015<1855:iadmro>2.0.co;2

Narita, D., Pochanart, P., Matsumoto, J., Someno, K., Tanimoto, H., Hirokawa, J., et al. (1999). Seasonal variation of carbon monoxide at remote sites in Japan. *Chemosphere*, *1*(1-3), 137–144. https://doi.org/10.1016/s1465-9972(99)00023-9

Ohara, T., Akimoto, H., Kurokawa, J. -I., Horii, N., Yamaji, K., Yan, X., & Hayasaka, T. (2007). An Asian emission inventory of anthropogenic emission sources for the period 1980–2020. *Atmospheric Chemistry and Physics*, *7*(16), 4419–4444. https://doi.org/10.5194/acp-7-4419-2007

Okamoto, S., & Tanimoto, H. (2016). A review of atmospheric chemistry observations at mountain sites. *Progress in Earth and Planetary Science*, *3*. https://doi.org/10.1186/s40645-016-0109-2(1)

Oltmans, S. J., Lefohn, A. S., Shadwick, D., Harris, J. M., Scheel, H. E., Galbally, I., et al. (2013). Recent tropospheric ozone changes—A pattern dominated by slow or no growth. *Atmospheric Environment*, *67*, 331–351. https://doi.org/10.1016/j.atmosenv.2012.10.057

Parrish, D. D., Law, K. S., Staehelin, J., Derwent, R., Cooper, O. R., Tanimoto, H., et al. (2012). Long-term changes in lower tropospheric baseline ozone concentrations at northern mid-latitudes. *Atmospheric Chemistry and Physics*, *12*(23), 11,485–11,504. https://doi.org/10.5194/acp-12-11485-2012

Pochanart, P. (2015). Residence time analysis of photochemical buildup of ozone in central eastern China from surface observation at Mt. Tai, Mt. Hua, and Mt. Huang in 2004. *Environmental Science and Pollution Research*, *22*(18), 14,087–14,094. https://doi.org/10.1007/s11356-015-4642-0

Pochanart, P., Akimoto, H., Maksyutov, S., & Staehelin, J. (2001). Surface ozone at the Swiss Alpine site Arosa: The hemispheric background and the influence of large-scale anthropogenic emissions. *Atmospheric Environment*, *35*(32), 5553–5566. https://doi.org/10.1016/s1352-2310(01)00236-9

Rayner, N. A., Parker, D. E., Horton, E. B., Folland, C. K., Alexander, L. V., Rowell, D. P., et al. (2003). Global analyses of sea surface temperature, sea ice, and night marine air temperature since the late nineteenth century. *Journal of Geophysical Research*, *108*(D14), 4407. https://doi.org/10.1029/2002JD002670

Shin, H. J., Park, J. H., Park, J. S., Song, I. H., Park, S. M., Roh, S. A., et al. (2017). The long term trends of tropospheric ozone in major regions in Korea. *Asian Journal of Atmospheric Environment*, *11*(4), 235–253. https://doi.org/10.5572/ajae.2017.11.4.235

Stein, A. F., Draxler, R. R., Rolph, G. D., Stunder, B. J. B., Cohen, M. D., & Ngan, F. (2015). NOAA's HYSPLIT atmospheric transport and dispersion modeling system. *Bulletin of the American Meteorological Society*, *96*(12), 2059–2077. https://doi.org/10.1175/BAMS-D-14-00110.1

Tanimoto, H. (2009). Increase in springtime tropospheric ozone at a mountainous site in Japan for the period 1998-2006. *Atmospheric Environment*, *43*(6), 1358–1363. https://doi.org/10.1016/j.atmosenv.2008.12.006

Tanimoto, H., Mukai, H., Sawa, Y., Matsueda, H., Yonemura, S., Wang, T., et al. (2007). Direct assessment of international consistency of standards for ground-level ozone: Strategy and implementation toward metrological traceability network in Asia. *Journal of Environmental Monitoring*, *9*(11), 1183–1193. https://doi.org/10.1039/b701230f

Tanimoto, H., Ohara, T., & Uno, I. (2009). Asian anthropogenic emissions and decadal trends in springtime tropospheric ozone over Japan: 1998–2007. *Geophysical Research Letters*, *36*, L23802. https://doi.org/10.1029/2009GL041382

Trenberth, K. E. (1984). Signal versus noise in the southern oscillation. *Monthly Weather Review*, *112*(2), 326–332. https://doi.org/10.1175/1520-0493(1984)112<0326:svnits>2.0.co;2

Verstraeten, W. W., Neu, J. L., Williams, J. E., Bowman, K. W., Worden, J. R., & Boersma, K. F. (2015). Rapid increases in tropospheric ozone production and export from China. *Nature Geoscience*, *8*(9), 690–695. https://doi.org/10.1038/ngeo2493

Wada, A., Matsueda, H., Murayama, S., Taguchi, S., Hirao, S., Yamazawa, H., et al. (2013). Quantification of emission estimates of CO_2, CH_4 and CO for East Asia derived from atmospheric radon-222 measurements over the western North Pacific. *Tellus B*, *65*(1), 18,037–18,015. https://doi.org/10.3402/tellusb.v65i0.18037

Wesely, M. L., & Hicks, B. B. (2000). A review of the current status of knowledge on dry deposition. *Atmospheric Environment*, *34*(12-14), 2261–2282. https://doi.org/10.1016/s1352-2310(99)00467-7

Wilcoxon, F. (1945). Individual comparisons by ranking methods. *Biometric Bulletin*, *1*(6), 80–83. https://doi.org/10.2307/3001968

Young, P. J., Naik, V., Fiore, A. M., Gaudel, A., Guo, J., Lin, M. Y., et al. (2018). Tropospheric ozone assessment report: Assessment of global-scale model performance for global and regional ozone distributions, variability, and trends. *Elementa: Science of the Anthropocene*, 6(1), 10. https://doi.org/10.1525/elementa.265